3.7 Supporting Information

3.7.1 Oxalic Acid: A Literature-Based Appraisal. Oxalic acid is the only organic substrate listed in Table 3.1 where complex formation constants with Mn^{III} are available. In addition, Mn^{III}-oxalate complexes have been synthesized and rate constants for their decomposition via intramolecular electron transfer have been measured. Using this information, we can place constraints on the possible pathways and rates of oxalic acid reaction with MnOOH.

Adsorption, i.e., the formation of a precursor complex, is the first step to any surface chemical reaction. The exact nature of this precursor complex is not at present known. Precursor complex formation may be outer-sphere or inner-sphere. Inner sphere complexes may be either monodentate or bidentate (coordination via one or both Lewis Base groups). Bidentate complexes may be mononuclear (involving only one surface-bound Mn^{III} atom) or binuclear (oxalate may bridge between neighboring Mn^{III} atoms).

Two competitive parallel processes are possible subsequent to the adsorption step: reductive dissolution and ligand assisted dissolution. In reductive dissolution, electron transfer from adsorbed oxalate to surface-bound Mn^{III} atoms, takes place, followed by release of Mn^{II} and oxidized organic substrate. (In the present case, oxalic acid is oxidized to inorganic carbonate species.) In ligand-assisted dissolution, adsorbed oxalate molecules detach surface-bound Mn^{III} atoms, yielding Mn^{III}-oxalate complexes in solution. Subsequent intramolecular electron transfer within these Mn^{III}-oxalate complexes would ultimately yield the same products as reductive dissolution, i.e., Mn^{II} and oxidized organic substrate.

The literature available to us has little to say about the reductive dissolution process. Instead, we focus our attention on ligand-assisted dissolution. Our first requirement is a solubility product constant for MnOOH(manganite). Combining the reported chemical potential of -557.7 kJ/mole for this solid *(1)* with chemical potentials for solute species *(2)* yields:

$$MnOOH(s) + 3H^+ + e^- = Mn^{2+}(aq) + 2H_2O \qquad \Delta G^o = -144.6 \text{ kJ/mole} \quad (1)$$

Next, ΔG^o for the following half-reaction is necessary:

$$Mn^{3+}(aq) + e^- = Mn^{2+}(aq) \quad E^0 = +1.57 \text{ volts} \qquad \Delta G^o = -151.5 \text{ kJ/mole} \quad (2)$$

This E^o value was supplied by James J. Morgan (pers. commun.), supported in part by two recent publications *(3, 4)*. Subtracting Reaction 2 from Reaction 1 allows us to calculate the solubility product constant:

$$MnOOH(s) + 3H^+ = Mn^{3+}(aq) + 2H_2O \qquad {}^*K_{so} = 10^{-1.20} \quad \Delta G^o = +6.89\text{kJ/mole} \quad (3)$$

We will denote the fully protonated form of oxalic acid as $H_2L^0(aq)$. The following equilibrium constants are available *(5)*:

$$H_2L^0(aq) = HL^- + H^+ \qquad K_{a1} = 10^{-1.25} \ (25^oC, 0.0 \text{ I}) \quad (4)$$

$$HL^- = L^{2-} + H^+ \qquad K_{a2} = 10^{-4.266} \ (25^oC, 0.0 \text{ I}) \quad (5)$$

$$Mn^{3+}(aq) + H_2O = MnOH^{2+} + H^+ \qquad {}^*K_1 = 10^{+0.43} \ (25^oC, 3.0 \text{ I}) \quad (6)$$

$$Mn^{3+} + L^{2-} = Mn^{III}L^+ \qquad K_1 = 10^{9.98} \ (25^oC, 2.0 \text{ I}) \quad (7)$$

$$Mn^{3+} + 2L^{2-} = Mn^{III}L_2^- \qquad \beta_2 = 10^{16.57} \ (25^oC, 2.0 \text{ I}) \quad (8)$$

$$Mn^{3+} + 3L^{2-} = Mn^{III}L_3^{3-} \qquad \beta_3 = 10^{19.42} \ (25^oC, 2.0 \text{ I}) \quad (9)$$

Infinite Dilution Scale constants (i.e., Reactions 4 and 5), in combination with the Davies Equation allow us to make activity corrections for experiments performed at any ionic strength below 0.5 M. Unfortunately, the only equilibrium constants available to us for

Reactions 6-9 are at high ionic strengths, making any attempts at ionic strength corrections provisional. Calculations based on these equilibrium constants are sufficient, however, for us to discern gross trends.

To construct the upper two plots of Figure S3.1, we have disallowed redox reactions. We treat oxalic acid as simply a chelating agent, and obtain dissolved Mn^{III} concentrations at equilibrium under the conditions specified. $TOTMn^{III}$ (total added Mn^{III}) is set at 200 μM. In the upper left plot, L_T (total added oxalic acid) is set at 5.0 mM; complete dissolution is achieved at pH values less than 5.3. $[Mn^{III}L_3^{3-}]$ is three-times larger than $[Mn^{III}L_2^{-}]$ and 50,000-times larger than $[Mn^{III}L^{+}]$ within the pH range shown. In the upper right plot, the pH is fixed at 5.0 and L_T is varied. 2.5 mM L_T is required for complete MnOOH dissolution to occur. $Mn^{III}L^{+}$ is the predominant species when $L_T < 0.32$ μM, $Mn^{III}L_2^{-}$ is the predominant species within the range 0.32 μM $< L_T <$ 1.7 mM, and $Mn^{III}L_3^{3-}$ is the predominant species at L_T values greater than 1.7 mM. We can conclude that oxalic acid is a strong enough chelating agent to yield substantial concentrations of dissolved Mn^{III}, but only at the highest oxalic acid concentrations (5 mM) and lowest pH values (below approx. 5.3) employed in our experiments.

Taube *(6)* presented the first quantitative description of the breakdown of Mn^{III}-oxalate complexes in solution via intramolecular electron transfer:

$$[Mn^{III}(L)_n]^{3-2n} \rightarrow Mn^{2+} + (n-1)L^{2-} + CO_2(aq) + CO_2^{\cdot-} \quad \text{where } n = 1, 2, 3 \qquad (10)$$

This first work, and two later publications by other authors *(7)*, have addressed whether the carbonate radical product ($CO_2^{\cdot-}$) is consumed primarily by recombination (regenerating free oxalate ion) or by fast oxidation by a second Mn^{III}-oxalate complex. If

we assume that the latter is predominant, then a modification of the rate equation presented by Taube *(6)* gives us the production rate for dissolved Mn^{II}:

$$dMn^{II}(aq)/dt = 2k_1[Mn^{III}L^{+}] + 2k_2[Mn^{III}L_2^{-}] + 2k_3[Mn^{III}L_3^{3-}] \quad (11)$$

where $k_1 = 1.97x10^{-1}\ s^{-1}$, $k_2 = 7.7x10^{-4}\ s^{-1}$, and $k_3 = 3.42x10^{-4}\ s^{-1}$ in 2.0 M KCl.

The following calculation is conveniently made. First, we assume that concentrations of 1:1, 1:2, and 1:3 mM Mn^{III}-oxalate concentrations are fixed by the MnOOH solubility constraints already described. Second, we assume that conversion of dissolved Mn^{III} to dissolved Mn^{II} does not alter the total dissolved Mn^{III} concentration, since Mn^{III}-oxalate species are continually replenished by ligand-assisted dissolution of MnOOH. The increase in total dissolved manganese ($Mn_T(aq)$) is tied directly to the production of dissolved Mn^{II} in accordance with Equation 11.

Figure S3.1 (c) and (d) show the results of this calculation when the oxalic acid concentration is fixed at 5.0 mM. Relative concentrations of $Mn^{III}L^{+}$, $Mn^{III}L_2^{-}$, and $Mn^{III}L_3^{3-}$ are constant below pH 5.3, the pH required for the complete dissolution of 200 μM MnOOH. As a consequence, $dMn^{II}(aq)/dt$ is fixed at 647 μM/hr. Above pH 5.3, $dMn^{II}(aq)/dt$ decreases more than750-fold for every unit increase in pH.

For comparison with the oxalic acid experimental results from Figure 3.6, a separate calculation was performed for 200 μM MnO_2 and 200 μM oxalic acid, covering the range $4.3 < pH < 6.9$ (Figure S3.2). This MnO_2 loading yields a $TOTMn^{III}$ equal to 44 μM. We will assume that this Mn^{III} component yields a solubility product constant that is identical to that of MnOOH. Again, we will assume that the ligand-assisted dissolution surface-bound Mn^{III} into $Mn^{III}L^{+}$, $Mn^{III}L_2^{-}$, and $Mn^{III}L_3^{3-}$ is instantaneous. Using this lower concentration, complete dissolution of Mn^{III} does not take place,

regardless of pH. (Mn^{III}(aq) is calculated to be 6.5 μM at pH 4.3 and 2.0×10^{-7} μM at pH 6.9). Throughout the pH range examined, the calculated rate is less than the experimentally-determined rate of Mn^{II}(aq) production. For every log unit increase in pH, dMn^{II}(aq)/dt decreases nearly 5000-fold.

3.7.2 Effect of Metal Ion Addition on Reductive Dissolution of MnO_2. As shown in Figure S3.3, adding Ca^{II}, Ni^{II}, and Zn^{II} at the onset of reaction decreased the initial rate of MnO_2 reduction by oxalic acid. The extent of rate inhibition depended upon the specific metal ion added as well as the added metal ion concentration. 0.1 and 0.2 mM Ca^{II} both decreased dMn^{II}(aq)/dt by about 25%. 0.5 mM Ca^{II} decreased the rate by approximately 90%, and 5.0 mM Ca^{II} shut down the dissolution reaction. With Ni^{II} and Zn^{II}, dMn^{II}(aq)/dt decreased gradually as metal ion concentrations were increased, but not in a linear fashion. 0.1 mM Ni^{II} decreased the rate by approximately 70 %, 0.2 mM Ni^{II} decreased the rate by approximately 80 %, and 5.0 mM Ni^{II} shut down the dissolution reaction. Ca^{II}, Ni^{II}, and Zn^{II} additions also decreased the initial rate of MnO_2 reduction by phosphonoformic acid (Figure S3.4). Generally, MnO_2 reduction by phosphonoformic acid is more tolerant to metal ion addition than MnO_2 reduction by oxalic acid, especially when the metal ion concentration is high.

Redox-inert metal ion additives can interfere with dissolved Mn^{II} production in a number of ways. (i) Metal ion additives may compete with organic substrate molecules for surface sites, and thereby interfere with formation of the surface precursor complex. Literature regarding +II metal ion adsorption onto low crystallinity Mn^{IV} (hydr)oxides has recently been compiled by Tonkin et al. *(8)*. At pHs at and below the "adsorption edge", extents of adsorption decrease in the order $Zn^{II} \geq Ni^{II} > Ca^{II}$, consistent with Ca^{II}

being the least inhibitory metal ion. (ii) Metal ion additives may form dissolved complexes with organic substrates, thereby interfering with surface precursor complex formation and with organic substrate-assisted detachment of surface-bound Mn^{II} product. The upper plots in Figures S3.3 and S3.4 calculated organic substrate solution in Mn (hydr)oxide-free solutions as a function of the concentrations of Ca^{II}, Ni^{II}, and Zn^{II}. (It should be noted that the formation of solid phases of any kind were ignored in this calculation.) For all three metal ions, the fraction of phosphonoformic acid in the free form is higher than the comparable fraction for oxalic acid. This finding is consistent with the greater inhibitory effect on metal ion addition to reactions involving oxalic acid. (iii) Metal ion additives may form precipitates with the organic substrate which are unavailable for reaction with the Mn (hydr)oxide surface. Solubility product constants have been reported for calcium oxalate solids *(5)* and for zinc oxalate solids *(9)*. When these solids are considered in the calculations shown in Figure S3.3, calcium oxalate precipitates when 0.1 mM Ca^{II} has been added, and zinc oxalate precipitates when 0.4 mM Zn^{II} has been added. By analogy, nickel oxalate solids must also exist, even though their solubility product constants have not been reported. Although no information is available regarding metal ion-phosphonoformate precipitates, they also potentially exist.

3.7.3 Time Course Plots for the Reaction of Phosphonoformic Acid with MnO_2. Our data analysis emphasize initial rates of reaction. Long-range time course behavior also provides important clues regarding dissolution mechanisms. In Figure S3.5, dissolved Mn^{II}(aq) production at pH 5.0, 6.0, and 7.0 is shown for the reduction of 200 μM MnO_2 by 5.0 mM phosphonoformic acid. At pH 5.0, Mn^{II}(aq) continues to increase throughout the time course shown. At pH 6.0, Mn^{II}(aq) prematurely reaches a plateau at

125 μM Mn^{II}(aq). This value exceeds $TOTMn^{III}$ in the system (44 μM). At pH 7.0, the plateau is reached when Mn^{II}(aq) reaches 91 μM. The mechanism responsible for this plateau phenomenon is not known.

References

(1) Bricker, O. Some stability relations in system Mn-O_2-H_2O at 25 degrees and 1 atmosphere total pressure. *Am. Mineral.* **1965**, 50, 1296-1354.

(2) Robie, R. A., Hemingway, B. S., and Fisher, J. R. *Thermodynamic Properties of Minerals and Related Substances at 298.15 K and 1 bar (105 pascals) Pressure and at Higher Temperatures.* U.S. Geological survey bulletin 1452. 1979, Washington, DC.

(3) Klewicki, J. K. and Morgan, J. J. Dissolution of β–MnOOH particles by ligands: Pyrophosphate, ethylenediaminetetraacetate, and citrate. *Geochim. Cosmochim. Acta* **1999**, 63, 3017-3024.

(4) Morgan, J. J. Manganese in natural waters and earth's crust: Its availability to organisms. In *Metal Ions in Biological Systems*, H. Sigel, Editor. 2000, Dekker: New York. 1-34.

(5) Martell, A. E., Smith, R. M., and Motekaitis, R. J. *NIST Critically Selected Stability Constants of Metal Complexes Database*. 2004, US Department of Commerce, National Institute of Standards and Technology: Gaithersburg, MD.

(6) Taube, H. The interaction of manganic ion and oxalate - rates, equilibria and mechanism. *J. Am. Chem. Soc.* **1948**, 70, 1216-1220.

(7) Jones, T. J. and Noyes, R. M. Mechanistic details of the oxidation of oxalate by maganese(III). *J. Phys. Chem.* **1983**, 87, 4686-4689.

(8) Tonkin, J. W., Balistrieri, L. S., and Murray, J. W. Modeling sorption of divalent metal cations on hydrous manganese oxide using the diffuse double layer model. *Applied Geochemistry* **2004**, 19, 29-53.

(9) KubackyBeard, U., Casey, W. H., Castles, J. J., and Rock, P. A. Standard gibbs energies of formation of $ZnC_2O_4 \cdot 2H_2O$(s), $CdC_2O_4 \cdot 3H_2O$(s), $Hg_2C_2O_4$(s), and PbC_2O_4(s) at 298 K and 1 bar. *Geochim. Cosmochim. Acta* **1996**, 60, 1283-1289.

(10) Packter, A. and Chauhan, P. The precipitation of alkaline-earth metal and transition metal oxalates from aqueous solution. Induction periods and nucleation rates. *Kristall and Technik* **1975**, 10, 621-631.

(11) Vincze, L. Determination of stability constants and individual quantum yields of iron(III)-glyoxylate complexes. *Hungarian J. Ind. Chem.* **1999**, 27, 241-244.

(12) Wang, Y. and Stone, A. T. The citric acid-$Mn^{III,IV}O_2$(birnessite) reaction. Electron transfer, complex formation, and autocatalytic feedback. *Submitted to Geochim. Cosmochim. Acta* **2005**.

Table S3.1. Capillary Electrophoresis Methods for Analytes in Organic Oxidation Experiments and Adsorption Experiments.

Reaction system	Analyte	Migration Time (min)	Detection Limit (μM)	Detection Wavelength (nm)	CE Electrolyte
glyoxylic acid + MnO_2 (or MnOOH)	glyoxylic acid	2.35	5	200	pH 5.4
	formic acid	2.01	2	200	5 mM 2-sulfobenzoic acid, 0.25 mM TTAB
oxalic acid + MnO_2 (or MnOOH)	oxalic acid	3.58	5	190	pH 7.1 25 mM pyrophosphate, 0.4 mM TTAB[b]
PFA + MnO_2 (or MnOOH)	PFA	2.95	5	200	pH 7.8
	orthophosphate	3.60	5	200	5 mM phthalic acid, 12.5 mM Tris, 0.25 mM TTAB
pyruvic acid + MnO_2 (or MnOOH)	pyruvic acid	1.68	5	200	pH 5.0
	acetic acid	1.89	5	200	5 mM benzoic acid, 0.25 mM TTAB
2,3-butanedione + MnO_2 (or MnOOH)	acetic acid	1.89	5	200	pH 5.0 5 mM benzoic acid, 0.25 mM TTAB
adsorption onto MnO_2	acetic acid			200	pH 7.8
	methylphosphonic acid			200	5 mM phthalic acid, 12.5 mM Tris, 0.25 mM TTAB

Table S3.2. logK Values Used to Perform Equilibrium Calculations.

Reactions	log ^{c}K	Ref.[a]	Ionic Str. (M)	T (^{o}C)
Reactions Involving Oxalic Acid				
$H^+ + L^{2-} = HL^-$	4.08		0.01	25
$2H^+ + L^{2-} = H_2L^0$	5.24		0.01	25
$Ca^{2+} + L^{2-} = CaL^0$	2.83		0.01	25
$Ca^{2+} + L^{2-} + H_2O = CaL{\cdot}H_2O$ (s)	8.39		0.01	25
$Ca^{2+} + L^{2-} + 3H_2O = CaL{\cdot}3H_2O$ (s)	7.96		0.01	25
$Ni^{2+} + L^{2-} = NiL^0$	4.80		0.01	25
$Ni^{2+} + 2L^{2-} = NiL_2^{2-}$	8.10		0.01	25
$Ni^{2+} + L^{2-} = NiL$ (s)	5.47	*(10)*		25
$Zn^{2+} + L^{2-} = ZnL^0$	4.51		0.01	25
$Zn^{2+} + 2L^{2-} = ZnL_2^{2-}$	7.33		0.01	25
$Zn^{2+} + L^{2-} + 2H_2O = ZnL{\cdot}2H_2O$ (s)	8.89	*(9)*		25
$Mn^{3+} + L^{2-} = MnL^+$	9.98		2.0	25
$Mn^{3+} + 2L^{2-} = MnL_2^-$	16.57		2.0	25
$Mn^{3+} + 3L^{2-} = MnL_3^{3-}$	19.42		2.0	25
Reactions Involving PFA				
$H^+ + L^{3-} = HL^{2-}$	7.96		0.01	25
$2H^+ + L^{3-} = H_2L^-$	11.83		0.01	25
$3H^+ + L^{3-} = H_3L^0$	13.66		0.01	25
$Ca^{2+} + L^{3-} = CaL^-$	4.36		0.01	25
$Ca^{2+} + H^+ + L^{3-} = CaHL^0$	10.58		0.01	25
$Ni^{2+} + L^{3-} = NiL^-$	6.18		0.01	25
$Ni^{2+} + H^+ + L^{3-} = NiHL^0$	11.30		0.01	25
$Zn^{2+} + L^{3-} = ZnL^-$	6.60		0.01	25
$Zn^{2+} + H^+ + L^{3-} = ZnHL^0$	11.63		0.01	25
Reactions Involving Glyoxylic acid				
$H^+ + L^- = HL^0$	3.37		0.01	25
$Fe^{3+} + L^- = FeL^{2+}$	3.10	*(11)*	0.01	25
$Fe^{3+} + 2L^- = FeL_2^+$	5.45	*(11)*	0.01	25
$Fe^{3+} + 3L^- = FeL_3^0$	6.20	*(11)*	0.01	25
$Fe^{3+} + 4L^- = FeL_4^-$	7.10	*(11)*	0.01	25
Metal Ion Hydrolysis Reactions				
$Ca^{2+} + H_2O - H^+ = Ca(OH)^+$	-12.79		0.01	25
$Ni^{2+} + H_2O - H^+ = Ni(OH)^+$	-9.98		0.01	25
$Ni^{2+} + 2H_2O - 2H^+ = Ni(OH)_2^0$	-19.08		0.01	25
$Ni^{2+} + 3H_2O - 3H^+ = Ni(OH)_3^-$	-29.99		0.01	25
$4Ni^{2+} + 4H_2O - 4H^+ = Ni_4(OH)_4^{4+}$	-25.38		0.01	25
$Zn^{2+} + H_2O - H^+ = Zn(OH)^+$	-9.09		0.01	25

$Zn^{2+} + 2H_2O - 2H^+ = Zn(OH)_2^0$	-16.98		0.01	25
$Zn^{2+} + 3H_2O - 3H^+ = Zn(OH)_3^-$	-28.39		0.01	25
$Zn^{2+} + 4H_2O - 4H^+ = Zn(OH)_4^-$	-41.01		0.01	25
$2Zn^{2+} + H_2O - H^+ = Zn_2(OH)^{3+}$	-8.91		0.01	25
$4Zn^{2+} + 4H_2O - 4H^+ = Zn_4(OH)_4^{4+}$	-25.78		3.0	25
$Mn^{3+} + H_2O - H^+ = Mn(OH)^{2+}$	0.43		3.0	25
Metal (Hydr)oxide Solubility-Controlling Phases				
$Ca^{2+} + 2H_2O - 2H^+ = Ca(OH)_2$ (s) (Lime)	-32.80		0.01	25
$Ca^{2+} + 2H_2O - 2H^+ = Ca(OH)_2$ (s) (Portlandite)	-22.79		0.01	25
$Ni^{2+} + 2H_2O - 2H^+ = Ni(OH)_2$ (s) (Amorphous)	-12.98		0.01	25
$Ni^{2+} + 2H_2O - 2H^+ = Ni(OH)_2$ (s) (Crystal)	-10.88		0.01	25
$Zn^{2+} + 2H_2O - 2H^+ = Zn(OH)_2$ (s) (Amorphous)	-12.56		0.01	25
$Zn^{2+} + 2H_2O - 2H^+ = \beta$-$Zn(OH)_2$ (s)	-11.84		0.01	25
$Zn^{2+} + 2H_2O - 2H^+ = \beta_2$-$Zn(OH)_2$ (s)	-11.88		0.01	25
$Zn^{2+} + 2H_2O - 2H^+ = \gamma$-$Zn(OH)_2$ (s)	-11.82		0.01	25
$Zn^{2+} + 2H_2O - 2H^+ = \varepsilon$-$Zn(OH)_2$ (s)	-11.93		0.01	25
$Zn^{2+} + H_2O - 2H^+ = ZnO$ (s)	-11.23		0.01	25
$Mn^{3+} + 2H_2O - 3H^+ = MnOOH$ (manganite)	1.20	*(12)*		25

[a] Unless otherwise noted, values taken from ref. *(5)*.

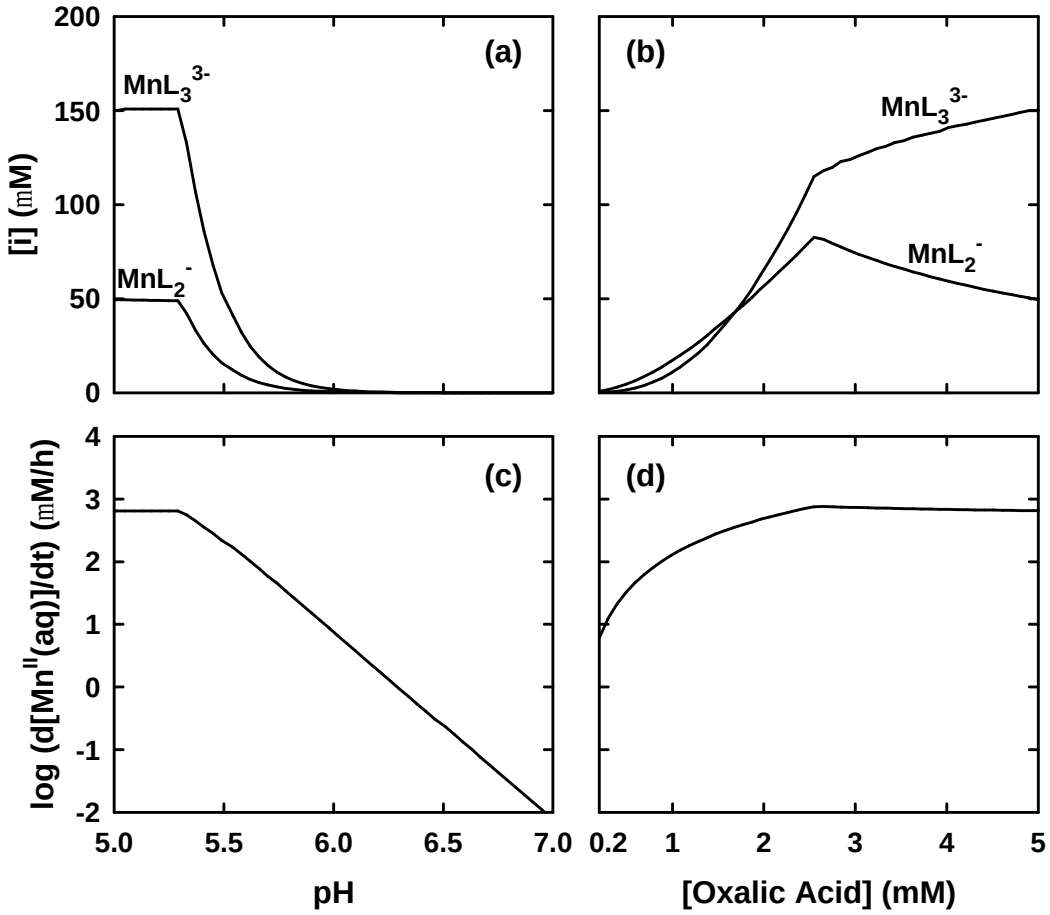

Figure S3.1. Calculations based upon the assumption that the ligand-assisted dissolution of 200 mM MnOOH(s) by oxalic acid (H_2L^0), yielding $Mn^{III}L^+$, $Mn^{III}L_2^-$, and $Mn^{III}L_3^{3-}$, is instantaneous. (a) Dissolved Mn^{III} speciation as a function of pH in the presence of 5.0 mM oxalic acid. (b) Dissolved Mn^{III} speciation as a function of oxalic concentration at pH 5.0. (c) and (d) Mn^{II} production rates under the conditions defined for plots (a) and (b), respectively.

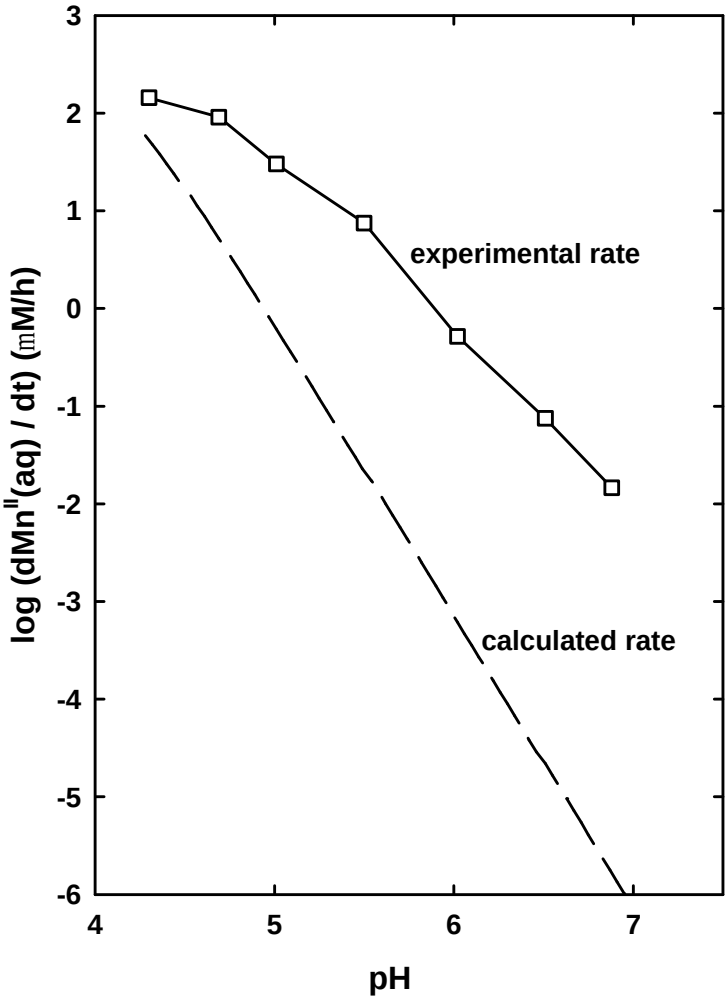

Figure S3.2. Experimentally-determined and calculated Mn^{II}(aq) production rates as a function of pH for reaction of 200 mM MnO_2 with 200 mM oxalic acid. Experimentally-determined rates were obtained from Figure 3.6 (refer to the figure for details). Calculated rates assume that the solubility product constant for the Mn^{III} component of MnO_2 particles is the same as for MnOOH (see text).

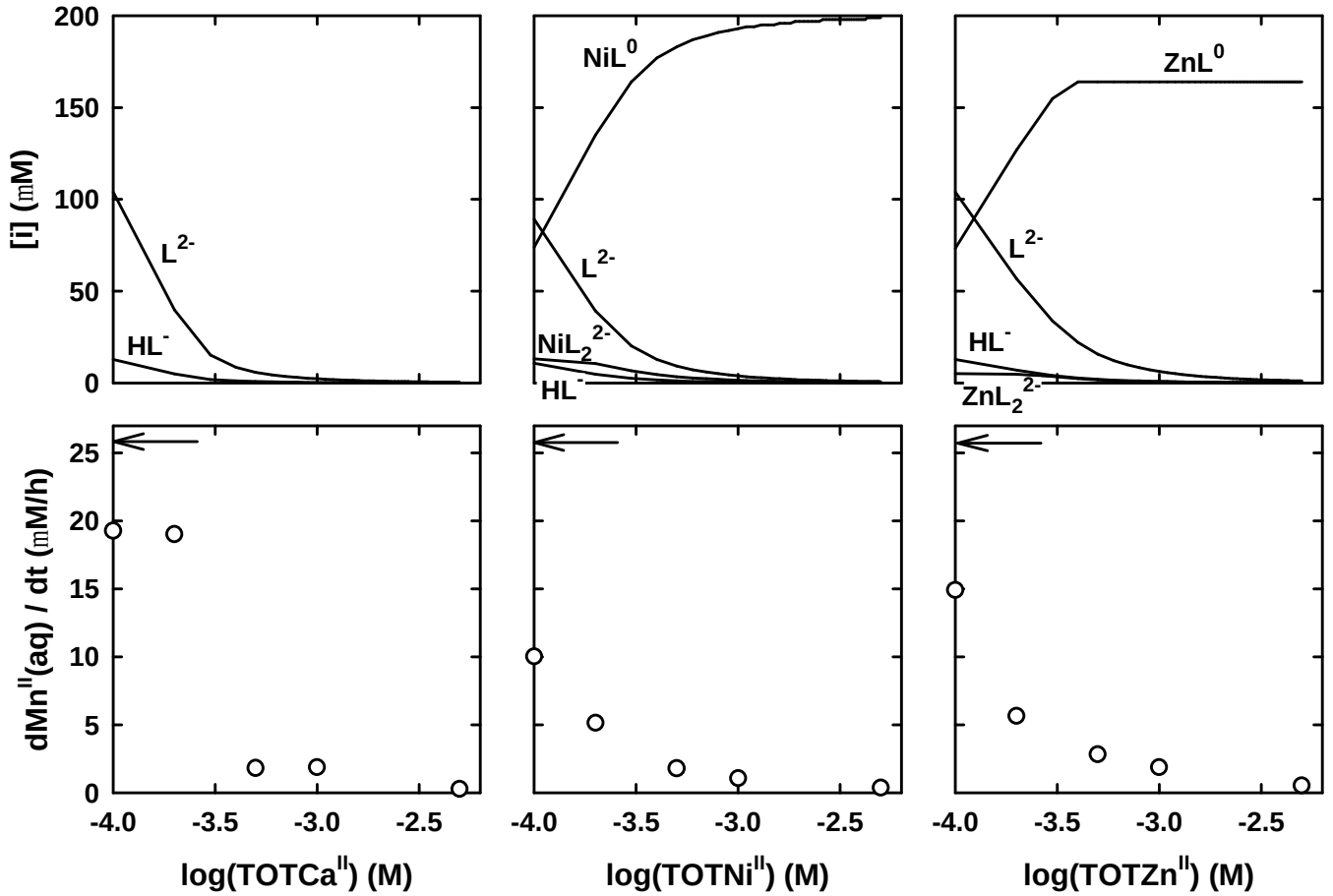

Figure S3.3. Top three panels: Calculated Ca^{II}, Ni^{II}, and Zn^{II} speciation in (hydr)oxide-free solutions containing 200 mM oxalic acid. The equilibrium constants listed in Table S3.1 were used. Bottom three panels: Effect of Ca^{II}, Ni^{II}, and Zn^{II} addition on the reaction of 200 mM oxalic acid with 200 mM MnO_2. Arrows denote $dMn^{II}(aq)/dt$ measured in metal additive-free suspensions.

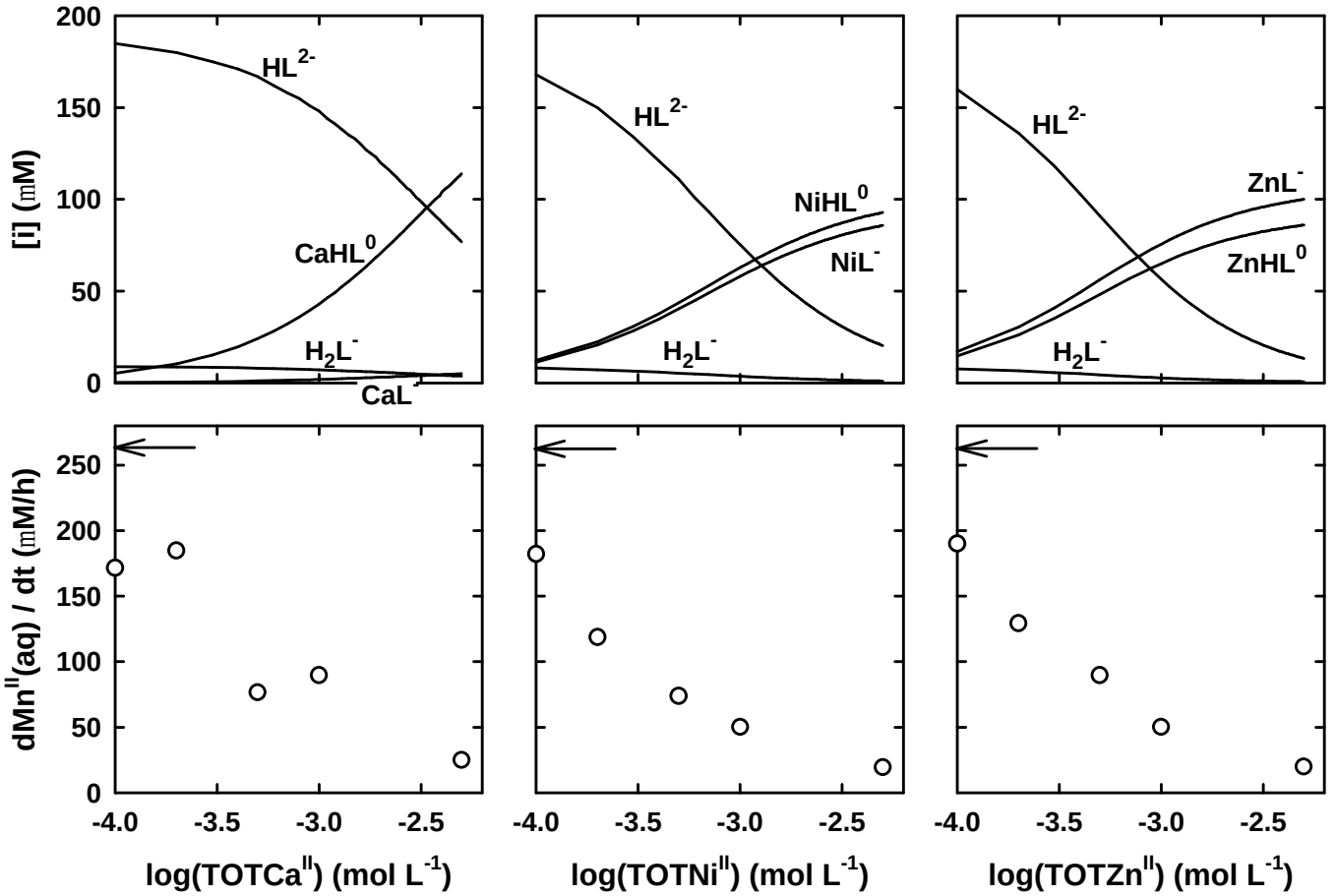

Figure S3.4. Top three panels: Calculated Ca^{II}, Ni^{II}, and Zn^{II} speciation in (hydr)oxide-free solutions containing 200 mM phosphonoformic acid. The equilibrium constants listed in Table S3.1 were used. Bottom three panels: Effect of Ca^{II}, Ni^{II}, and Zn^{II} addition on the reaction of 200 mM phosphonoformic acid with 200 mM MnO_2. Arrows denote $dMn^{II}(aq)/dt$ measured in metal additive-free suspensions.

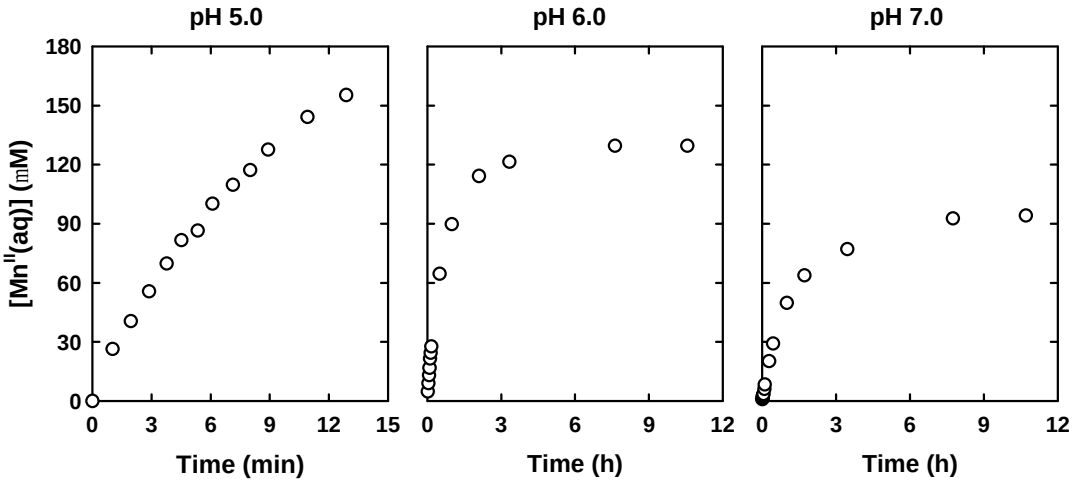

Figure S3.5. Time course plots for dissolution of 200 mM MnO_2 by 5.0 mM phosphonoformic acid at three different pHs. Constant pH was maintained using a pH stat.